Evaluation of Holistic Treatment for ALS Reveals Possible Mechanism and Therapeutic Potential

Andrea Lavado[1,†], Xiufang Guo[1,†], Alec ST Smith[1], Nesar Akanda[1], Candace Martin[1], Yunqing Cai[1], Dan Elbrecht[1], My Tran[1], Jean-Paul Bryant[1], Alisha Colon[1], Christopher J Long[1], Stephen Lambert[2], Dave Morgan[3], James J Hickman[1*]

[1] NanoScience Technology Center, University of Central Florida, 12424 Research Parkway, Suite 400, Orlando, FL 32826

[2] College of Medicine, Biomedical Science Program, University of Central Florida, 6850 Lake Nona Blvd. Orlando, Fl 32827

[3] USF Health Byrd Alzheimer Institute, Morsani College of Medicine, University of South Florida, 4001 E. Fletcher Ave., Tampa FL 33613

[†]Authors contributed equally to the work.

ABSTRACT

There has been a tremendous amount of research into the causes of Amyotrophic Lateral Sclerosis (ALS), but yet very few treatment options beyond amelioration of symptoms. A holistic approach has shown anecdotal evidence of slowing disease progression and this treatment, known as the Deanna Protocol (DP), postulates that ALS is a metabolic disease caused by glutamate that induces toxicity. In this study, glutamate exposure to human motoneurons was investigated and found not to significantly affect cell viability or electrophysiological properties. However, varicosities were observed in axons suggestive of transport impairment that was dose dependent for glutamate exposure. Surprisingly, a subset of the components of the DP eliminated these varicosities. To verify this finding a human SOD1 patient-derived iPSC line was examined and significant numbers of varicosities were present without glutamate treatment, compared to the iPSC control, indicating the possibility of a common mechanism despite different origins for the varicosities. Importantly, the DP ameliorated these varicosities by over 70% in the patient derived cells as well. These results are consistent with much of the literature on ALS and give hope for treatment not only for arresting disease progression using compounds considered safe but also the potential for restoration of function.

INTRODUCTION

Amyotrophic Lateral Sclerosis (ALS), also known as Lou Gehrig's disease, is characterized by a progressive neurodegeneration of upper and lower Motoneurons (MNs) in the brain and spinal cord (1, 2). The pathological features of this disease are spasticity, hyperreflexia, muscle weakness; atrophy and paralysis which ultimately results in death due to compromised respiratory functions (1, 3). Although the origins of ALS are still unclear, 5 to 10% of the cases have been associated with a hereditary form of the disease and 82% with a sporadic component (1-4). Previous research has indicated the process could proceed by Motoneuron (MN) death (5-7), loss of Neuromuscular Junctions (NMJs) by MN dysfunction (8-10) and the overexpression of NOGO in the contacted muscle (11, 12). Glial cells have also been implicated in certain studies where astrocytic dysfunction has been documented (13-16) as well as the activation of microglia that then proceeds to attack the CNS components of the NMJ (8, 17, 18). Inflammation has been targeted in one of the modes of microglia activation (19-23) but also has been postulated to cause slow degradation of the MNs (24). At the genetic level mutations in the genes for Superoxide Dismutase 1 (SOD1), TAR DNA-binding protein (TDP-43), fused in sarcoma/translated in liposarcoma (FUS/TLS), and more recently C9-ORF72 (25) have been suggested to contribute to MN degeneration (3, 26-28). These mutations have been proposed to primarily contribute by initiating protein misfolding, forming protein aggregates and insoluble inclusions but also by interfering with RNA regulation and processing (3, 28-31). Alterations in the retrograde transport of autophagosomes have also been identified in ALS patients, by mutations in dynein and dynactin genes, as well in the ubiquitin-proteasome pathway, with alterations in the ubiquilin2 (UBQLN2), optineurin (OPTN), P62, and Valosin-Containing Protein (VCP) genes, thus interfering with the general mechanism of protein degradation (3, 32-34). Glutamate excitotoxicity has also been reported as a hallmark of the disease (5, 6, 35, 36). However, there is no clear consensus on the cause or even the mechanisms that initiate and enable disease progression, especially in sporadic cases.

The therapeutics for ALS are limited, mainly due to this inherent complexity of the disease. Riluzole is the only FDA approved drug for treating ALS, however, its specific mechanism of action is not well understood and only limited improvement in motor function and lifespan are achieved (31, 37). A recent finding has targeted hyperexcitability using the drug Retigabine and it is in clinical trials (38). Additionally, a holistic metabolic therapeutic has

Citation: James J Hickman et al. Ijppr.Human, 2017; Vol. 11 (1): 348-374.

349

been highlighted, where anecdotal reports of patients utilizing a supplement cocktail DP suggested the effectiveness of the treatment as indicated by an improvement in motor function (1, 24). The DP is a collection of commercially available nutritional supplements, formulated by Vincent Tedone, a retired orthopedic surgeon. He developed the protocol for his daughter, Deanna when she was diagnosed with ALS. The major components of this protocol, including proposed biological activities of each component, was described previously (24). Studies in an ALS mouse model (hemizygous mice with transgenic expression of a G93A mutant form of human *SOD1* gene) supported the possible benefit of this metabolic therapy for improving motor function and for extending survival (1). The principle mode of action proposed for the DP is the targeting of metabolic pathways known to be altered in ALS and is based on supplements, such as arginine alpha-ketoglutarate (AAKG), Coenzyme Q10 (CoQ10), and γ- Aminobutyric acid (GABA) among others. This formulation was developed based on the literature to counteract oxidative metabolism, confer mitochondrial protection, glutamate detoxification and energy production, which are known to be altered in ALS pathology (1,24, 39). However, despite the positive feedback from anecdotal reports, no solid evidence has confirmed the effectiveness of these components in a human model, and no experiments have attempted to determine the actual mechanism of action or to optimize the protocol.

It has been postulated that the cause of this metabolic dysregulation is glutamate toxicity. Glutamate is one of the principal mediators of excitatory synaptic transmission in the mammalian nervous system. High extracellular concentrations of glutamate are normally concentrated in nerve terminals and are transient, extremely brief, and localized to the post-synaptic terminals, where they are necessary to mediate synaptic transmission (5, 7). Dysregulation of glutamate handling in the central and peripheral nervous systems leads to uncontrolled Ca^{2+} influx into neurons and secondary excitotoxicity (6). Additionally, prolonged exposure to elevated extracellular glutamate concentrations has been shown to lead to neuron dysfunction, damage, and death (5-7). Despite its suggested role in the progression of multiple neuropathic conditions, the exact mechanism of glutamate-induced neurotoxicity likely varies across different pathologies and in different neuronal subtypes. Studies from rodent cultures indicated that glutamate exposure induced distal axonopathies, characterized by axonal swellings and abnormal co-localization of phosphorylated and dephosphorylated neurofilament proteins at the terminal segment of axons. This was only observed in relatively aged (>3 weeks) MNs, but not in younger MNs or cortical neurons, but was not linked to

Citation: James J Hickman et al. Ijppr.Human, 2017; Vol. 11 (1): 348-374.

350

ALS in this study (40). However, this observation provides a strong link between hypertoxicity-induced axonopathy to the pathological cytoskeletal changes observed in ALS (41, 42). All these events provide a possible mechanism underlying the pathogenesis of ALS as it contributes to accumulation of cytotoxic species which are hypothesized as responsible for MN degeneration (32).

To investigate the relationship between glutamate toxicity to MNs and how the DP may be ameliorating those deficiencies, experiments were undertaken to examine the electrical properties of MNs after inducing glutamate toxicity. Interestingly this caused the appearance of distinct and quantifiable axonal features in cultured MNs treated with glutamate, and they are similar to defined pathological features in ALS (41, 42). Most interestingly, these varicosities were abolished by treatment with a subset of the metabolic protocol. These axonal features were also present in MNs derived from ALS patient induced Pluripotent Stem Cells (iPSCs) with the SOD1 mutation and the varicosities were also significantly reduced by the metabolic protocol compared to WT iPSCs. These experiments, while preliminary, have led us to propose a rationale for ALS progression based on the available literature as well as the suggestion of an overall mechanism for the disease. It also provides the first evidence in human *in vitro* systems of the possible benefits of the DP to support the anecdotal evidence in human patients.

MATERIALS AND METHODS

Surface modification:

The surfaces for culture of the Human motoneurons (HMNs) were modified with N-1[3-trimethoxysilyl) propyl] diethylenetriamine (DETA), a surface modification that has been previously shown to support neuronal growth. The surface modification and characterization were performed according to a protocol previously described by this group (43).

Cell culture:

Human spinal cord stem cell-derived motoneurons were prepared and cultured as detailed previously (44). The spinal cord stem cell line NSI566RSC was purchased from Neural Stem Inc. Passage 11 to 13 cells were used in this study. The induction procedure consisted of three steps. First, for proliferation, one aliquot of cryopreserved cells ($\sim 3 \times 10^6$ cells) was seeded into a T25 flask precoated with PDL in N2B medium with bFGF (10 ng/mL) in the presence

Citation: James J Hickman et al. Ijppr.Human, 2017; Vol. 11 (1): 348-374.

351

of fibronectin (1.5 μg/mL). The medium was changed every other day, while bFGF (10 ng/mL) was added on the days when media was not changed. The cells were proliferated for 6 to 8 days to roughly 80% confluency. Next, they were trypsinized and replated onto permanox dishes (60 mm, Nunc) coated with PDL and fibronectin at a density of 2×10^6 cells/dish. For MN induction, the stem cells were first treated in priming medium for 4 days with a half medium change on Day 2. They were then fed with MN differentiation medium (44) for the remainder of the culture period every 2 days by changing half of the medium. On day 10 in the dish, the differentiated cells were harvested with trypsin and replated onto DETA-coated glass coverslips with a density of 200 cells/mm^2. They were maintained for 10 days on coverslips in MN medium to ensure complete differentiation and functional maturation before any glutamate and/or DP treatments were initiated. The components of priming medium and human motoneuron medium are described as in (44). For glutamate experiments, 20 mM glutamate was added to the motoneuron differentiation medium and the solution was used to perform a half medium change, bringing the final concentration down to 10 mM. Cells were maintained in glutamate treated medium for 48 hours prior to analysis. Control cultures were treated similarly but with medium only.

Differentiation of MNs from human induced Pluripotent Stem Cells (hiPSCs):

MNs differentiated from iPSC lines isolated from an ALS patient with the SOD1 mutation (LEU144PRO) (line ND39032) and a healthy subject (line ND41865) were analyzed. The hiPSCs were obtained from the Coriell Institute established by the NIH and as received cells were counted as Passage 0. Cells were passaged up to P10 utilizing the established procedures recommended by NIH. Cells from P6~10 were used in this study for MN induction. MNs were differentiated from iPSCs based on the protocols of (45) with the modification of replacing Component C with LDN 193189 (0.1 μM) and SB431542 (6 μM).

Electrophysiological data acquisition and analysis:

The electrophysiological properties of treated and untreated stem cell derived MNs were investigated immediately after each glutamate and/or DP treatment protocol using whole-cell patch-clamp recording techniques as detailed previously (46). Briefly, cultured neurons maintained on glass coverslips were placed in the recording chamber of a Zeiss Axioscope 2FS Plus upright microscope. The motoneurons in culture were distinguished from non-neuronal cells visually using an infrared Differential Interference Contrast (DIC) video-

Citation: James J Hickman et al. Ijppr.Human, 2017; Vol. 11 (1): 348-374.

352

microscope. Large multipolar cells (15 to 20 μm in diameter) with bright somas were identified as MNs. Borosilicate glass patch pipettes (BF 150-86-10; Sutter Instrument Company), with a resistance of 6 to 10 MΩ, were made using a Sutter P97 pipette puller (Sutter Instrument Company). Both current-clamp and voltage-clamp recordings were taken using a Multiclamp 700A amplifier (Axon Instruments). The pipette (intracellular) solution contained 1 mM EGTA, 140 mM K-gluconate, 2 mM $MgCl_2$, 2 mM Na_2ATP and 10 mM HEPES (pH 7.2). The MN medium was supplemented with 10 mM HEPES (pH 7.2) and was used as the extracellular solution for all patch experiments.

Following the formation of a giga-Ω seal and membrane puncture, the cell capacitance was compensated. Signals were filtered at 3 kHz and sampled at 20 kHz using a Digidata 1322A interface (Axon Instruments). Data recording and analysis were performed using the pClamp8 software (Axon Instruments). Membrane potentials were corrected by subtraction of a 15 mV tip potential, which was calculated using Axon's pClamp8 program. Depolarization-evoked inward and outward currents were examined in voltage-clamp mode. Depolarization-evoked action potentials were examined in current-clamp mode and induced using 1 second depolarizing current injections from a -70 mV holding potential.

hMN Glutamate treatment:

To test glutamate excitotoxicity, hMNs on Day 10 after replating onto coverslips were treated with a solution of the described concentration L-glutamic acid monosodium (G1626 Sigma). To apply the experiments, 20 mM glutamate was added to the MN differentiation medium and the solution was used to perform a half medium change, bringing the final concentration down to 10 mM. Cells were maintained in glutamate treated medium for 48 hours prior to analysis. Control cultures were treated similarly but with medium only. At the end of the treatment, hMN on coverslips were subjected to immunocytochemistry.

Cell survival studies:

To determine cellular viability, glutamate treated and untreated hMNs were incubated for 2 hours at 37ºC with 1.2 mM of 2-(4,5-dimethylthiazol-2-yl)-2,5diphenyltetrazolim bromide (MTT) (Sigma- Aldrich) diluted in culture medium. Supernatant removal was followed by the addition of the solubilization reagent (0.57% acetic acid and 1% SDS in DMSO). Cell viability was determined at 570 nm in a Synergy HT plate reader and KC4 software. The

Citation: James J Hickman et al. Ijppr.Human, 2017; Vol. 11 (1): 348-374.

353

results were expressed as the percentage of cell survival relative to the control (untreated). Viability was determined after 48 hours glutamate treatment.

hMN treatment with Deanna protocol formulations:

To evaluate the effectiveness of DP based formulations, hMNs were treated according to the scheme described in Figure 3A. Little data exists for the serum concentration of each DP component in humans, and almost no data on the CNS concentration of the components so a brief dose response test was performed starting from the data in Supplemental Table S1 by incubating hMNs with each component for 48 hours and measuring hMN viability by MTT. A dosage that was high, but below that which caused MN viability loss, was utilized for experiments. The components and dosage of the DP treatment we utilized for hMN treatment are listed in Figure 3A. DP components were added to the hMN culture between D10-D12 simultaneously with glutamate, or between D13-D14 after the glutamate treatment was completed. Correspondent controls were included in which either glutamate treatment or DP components were omitted. The coverslips were then fixed for immunocytochemical analysis on D12 or D14 after the glutamate and/or DP treatments. The treatments were applied on day 10 after replating for MNs derived from spinal cord stem cells by including the respective components in fresh MN medium and administrated with a complete medium change. MNs derived from iPSCs were treated according to the treatment outlined above with the DP-2 between D12 to D14 after being replated onto coverslips.

Immunocytochemistry and Microscopy:

Cells were fixed with 4% paraformaldehyde for 15 minutes at room temperature and were then rinsed with 1x PBS two times. Cells were permeabilized for 10 minutes with 0.1% Triton X-100. Subsequently, cells were blocked for 1 hour at room temperature in blocking buffer (2.5% donkey serum + 2.5% goat serum + 1% BSA) and incubated with primary antibodies overnight at 4ºC. The coverslips were washed again with 1x PBS three times (5 minutes each wash) followed by the incubation with the secondary antibodies (1:250 diluted in blocking buffer) for 2 hours, at room temperature protected from light. They were then washed with 1x PBS (4 washes; 5 minutes each). Nuclear staining was performed by the addition of a DAPI solution (300 µM) for 10 minutes at room temperature. ProLong® Gold Antifade Mountant (P36930) was used to mount the coverslips onto slides. Primary antibodies utilized in this work include: Chicken-anti-neurofilament (Millipore, 1:1000),

Citation: James J Hickman et al. Ijppr.Human, 2017; Vol. 11 (1): 348-374.

354

mouse-anti-SMI32 (Calbiochem, 1:100), Rabbit-anti-GluR1 (Millipore, 1:100), Rabbit-anti-GluR2&3 (Millipore, 1:100), Goat-anti-ChAT (Millipore, 1:100), Rabbit-anti-β III Tubulin (Sigma, 1:1000), Rabbit-anti-MAP2 (Millipore, 1:1000). The monoclonal antibody against SV2 (mouse, 1:10) was obtained from the Developmental Studies Hybridoma Bank which is under the auspices of the NICHD and maintained by the University of Iowa. Secondary antibodies include: Goat-anti-Mouse-488, Goat-anti-Mouse-568, Goat-anti-chicken-568, Goat-anti-chicken-488, and Goat-anti-Rabbit-568. All the secondary antibodies were from Invitrogen. Fluorescence imaging was performed in an UltraView^{TM} spinning disk confocal system (PerkinElmer) with an AxioObserver Z1 (Carl Zeiss) stand, and a Plan- Apochromat objective 40x/0.75 air. Z-stack projections of the scanned images were processed and modified with Volocity software.

Quantification and statistical analysis:

For the quantification of the axonal varicosities, the cells were immunostained with neurofilament antibody and imaged by confocal microscopy. The images were analyzed with the software image J. The number of varicosities/μm at 40x magnification was calculated from the collected images. Total axonal length from each image was measured using image J and the number of varicosities/μm was quantified. At least 30 images were collected from each condition. Statistical analysis by one-way single factor ANOVA followed by Dunnett's test (alpha=0.05) was performed to compare differences between samples. The data were represented as the mean plus or minus the sample standard error of the mean (±SEM) of three or more independent biological repeats.

We show that the DP effectively reduces varicosities in two separate conditions: when the varicosities are caused by glutamate (as in the wild-type line), and when the varicosities are present without induction (as in the SOD1 mutant line). In this work, the paired nature of varicosity analysis blocks for differences in the underlying cell lines to isolate the effect of the drug treatment within these two conditions. By showing significant reductions in varicosities produced by two very different experimental protocols (induced and natively produced), we conclusively demonstrate that the DP-2 Deanna Protocol affects an underlying mechanism for varicosity production or prevention. Based on approximations of variance within SOD1 mutant lines and variation within the population as a whole, including both SOD1 mutant and spinal cord stem cell derived MN, adding additional mutant cell lines would only improve statistical confidence and decrease the minimum detectable difference

Citation: James J Hickman et al. Ijppr.Human, 2017; Vol. 11 (1): 348-374.

355

between means by approximately 5%. This small improvement is unnecessary considering the statistical power demonstrated in distinguishing changes among conditions in our data.

RESULTS

Cell viability assays of motoneurons exposed to glutamate

To mimic glutamate toxicity, a phenotype observed frequently in ALS pathology, hMNs differentiated from fetal spinal cord stem cells (SCSC) (44) were exposed to glutamate for 48 hours for increasing concentrations. An MTT assay was used to establish a correlation between glutamate dosage and cell viability (Figure 1A). The results obtained suggest that hMN viability was not affected by 48 hours of glutamate treatment for up to a concentration of 10 mM. Although a small decrease in viability was observed for dosages above 5 mM, the results were not significantly different from the untreated group (Treated [1-10 mM] vs. Untreated $P>0.01$).
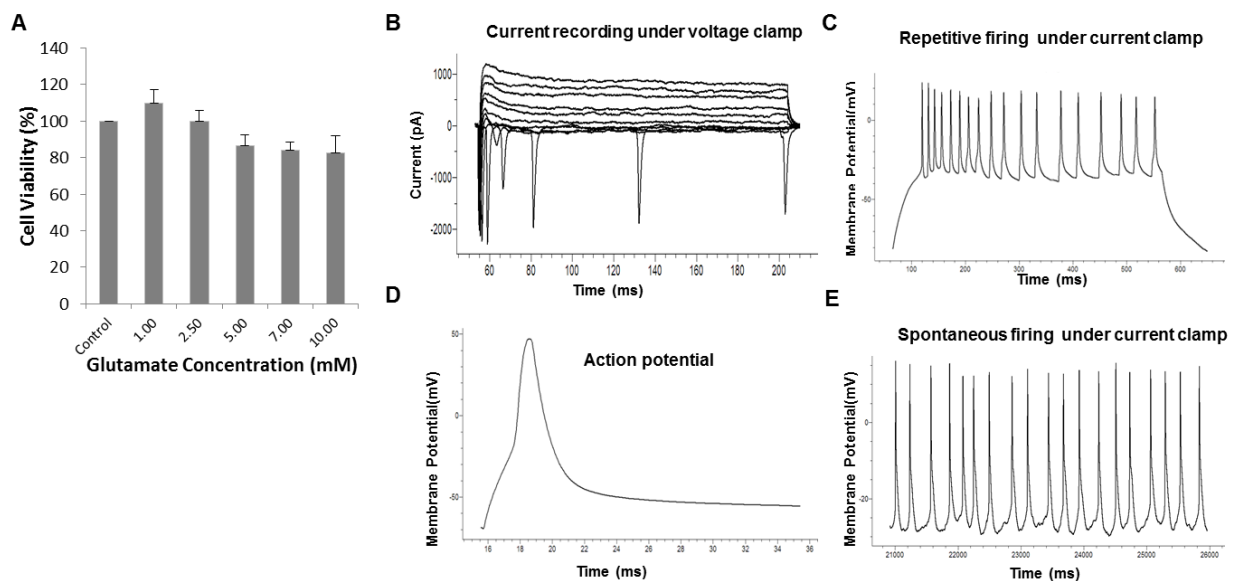

Figure 1. Neuronal viability and function after glutamate treatment. A) Viability of cultured hMNs upon 48 hours treatment with increasing concentrations of glutamate, analyzed with a MTT assay. No significant reduction in viability was observed (P>0.01). Data represent the mean ± S.E.M. **B-E)** Electrophysiological characterization of hMNs after 10 mM glutamate treatment. **F)** Analysis of the major electrophysiological parameters indicated MNs with and without glutamate treatment have similar electrophysiological function. Data represent the mean ± SD.

Citation: James J Hickman et al. Ijppr.Human, 2017; Vol. 11 (1): 348-374.

356

Electrophysiological properties of hMN cultures in response to glutamate treatment.

Patch clamp analysis highlighted minor alterations in hMN electrophysiological properties in response to 48-hour glutamate exposure (Figure 1B-E). First observation is that the resting membrane potential was less hyperpolarized in glutamate-treated MNs. Similarly, glutamate treated MNs exhibited smaller action potential amplitudes than control cells and there was a slight decrease in the number of cells that were capable of repetitive firing under depolarization. However, none of these differences were statistically significant (*P>0.01*). In addition, no significant differences were observed in the amplitudes of inward sodium and outward rectifying potassium currents from glutamate treated and untreated controls. Overall, given the severe dysfunction found in ALS MNs, the degree of functional deficits was relatively minor compared to what was expected (Table 1). In order to examine the possibility that the glutamate treatment would cause a functional deficit in MNs at later time periods, glutamate-treated MN cultures were analyzed by patch clamp again 4 days after the cessation of glutamate treatment. No significant difference was observed between the treated and untreated cultures over this time period (Supplemental Table S2). All these results indicate that 48 hours Glutamate treatment did not cause functional deficits which are detectable by the described analysis. To further evaluate the effect of glutamate on hMNs function, the expression of glutamate receptors in the hMNs and their response to glutamate was also confirmed in these SCSC-hMNs (Supplemental Figure S2).

Table 1. Analysis of the major electrophysiological parameters indicated no difference between MNs with and without Glutamate treatment. Data represent the mean +/- SD.

SCSC-MN	RP (mV)	AP (mV)	I Na+ (pA)	I K+ (pA)	Neurons w/ repetitive firing	Rate of Repetitive Firing (Hz)
Control	-48.82+/- 9.15	94.06+/- 8.34	-2087.6+/- 754.02	1590.09+/- 384.3	90%	15+/-6.4
Glutamate	-40.86+/- 4.88	82.88+/- 14.32	-2051.04+/- 901	1761.66+/- 903	66.7%	15.3+/-7.6

Morphological changes in response to glutamate treatment.

Morphological alterations in glutamate (10 mM, 48 hours) treated MN cultures 10 days after cell plating were also investigated by phase contrast microscopy. The formation of aberrant

Citation: James J Hickman et al. Ijppr.Human, 2017; Vol. 11 (1): 348-374.

357

axonal swellings or varicosities in the neurites were found as a consequence of glutamate treatment and not found for its untreated counterparts, as can be observed in Figures 2A and B. Additional characterization of the axonal swellings was performed by immunochemical labeling for neurofilament, which specifically stained neural axons. While few axonal swellings were observed in the control group (Figure 2C), numerous varicosities along the processes that were immunopositive to neurofilament were demonstrated in the glutamate exposed hMN culture (Figure 2D). From the literature, formation of axonal varicosities occurs as a response to multiple stimuli and stressors, including mechanical stress, axonal damage, heat and cold, toxins, and anesthetics (47-50) as well as in neurodegenerative diseases (51, 52). Human MNs derived from ALS patient iPSCs revealed neurofilament aggregation as an early ALS pathological event which underlies MN pathology (53). Electron microscopy analysis has revealed breakage of microtubules at the swelling locations, which caused disorganization of cytoskeletal proteins and accumulation of axoplasm membrane-bound bodies, vesicles, mitochondria and other cargo in the varicosities, which was linked to impairment of axonal transport (47, 48, 51, 52). Since disruptions of axonal transport of neurotransmitters and other critical biological materials necessary for synaptic function could severely affect MN communication, these cultures were co-stained with neurofilament and synaptic vesicle protein 2 (SV2) (Figure 2E and F). SV2 is a marker for synaptic vesicles (54), and the impaired transport of synaptic vesicles has been utilized as a reporter for axonal transportation deficits. Increased numbers of SV2 clusters were observed in glutamate treated cultures (Figure 2F), but not in untreated controls (Figure 2E), and a large number were co-localized with varicosities. This result indicates that synaptic vesicles, one of the normal cargos of axonal transport, were accumulated in these varicosities, strongly suggesting the impairment of axonal transport which correlates with the previous literature (51).

To further investigate the insult produced by glutamate treatment in hMNs, a dose dependent quantification of axonal varicosities was performed. The impact of glutamate exposure on the induction of morphologically aberrant axonal swellings was examined for hMNs 10 days after replating that were treated for 48 hours in a dose-dependent manner (Figure 2G). Neurofilament labeling was used to quantify the number of axonal varicosities formed. No significant effects were observed at low glutamate treatment, 1 mM (Treated [1 mM] vs. untreated $P>0.01$). However, the density of varicosities formed along the axonal network was found to significantly increase as the glutamate dosage increased (Figure 2H) (Treated [2.5-

Citation: James J Hickman et al. Ijppr.Human, 2017; Vol. 11 (1): 348-374.

358

10 mM] vs. untreated *P<0.01).* Glutamate dosages of 10 mM resulted in the highest number of axonal varicosities.
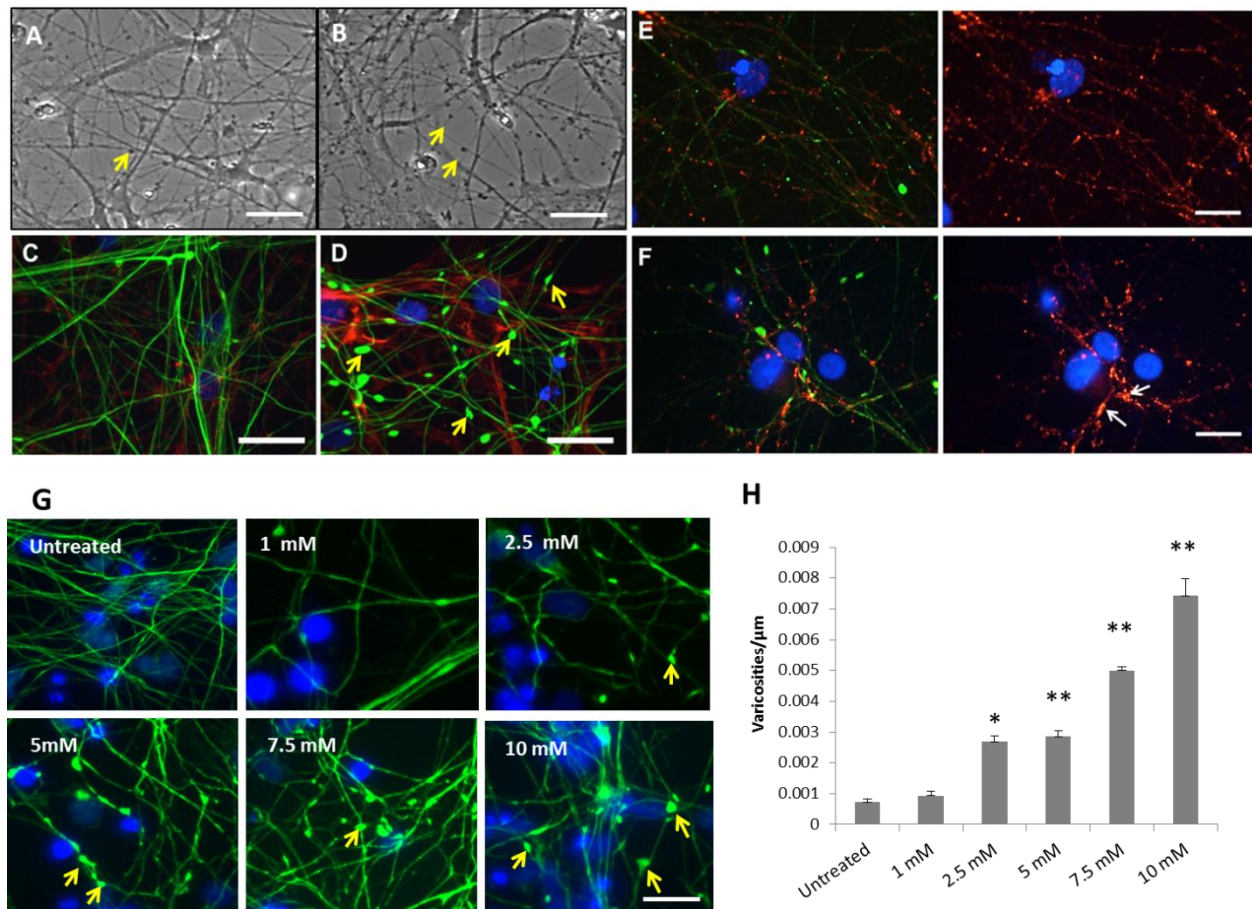

Figure 2. Assessment of morphological changes in response to glutamate treatment by phase microscopy and immunocytochemistry. **A&B)** The increase in axonal varicosities and the trend towards a reduction in axon density were observed after 48 hours of glutamate treatment (**B**) compared to those before treatment (**A**). Scale bar = 60 μm. **C&D)** Axonal morphology of MNs was visualized by immunocytochemistry with axonal marker NF (green) and co-stained for actin (red) and nuclei (Dapi, blue) in Control (**C**) and Glutamate treated (10 mM) (**D**) conditions. Note the formation of morphologically aberrant varicosities in the treated condition (swellings stained green). Selected varicosities are highlighted by yellow arrows. Scale bar = 30 μm. **E&F)** Untreated (**E**) and 10 mM glutamate treated (**F**) human motoneurons 10 days after plating were immunostained for neurofilament (green), SV2 (red) and nuclei (blue). Panels on the left and right show the same field of view with and without neurofilament respectively, in order to accentuate the SV2 clustering observed in glutamate treated cultures. Scale bar = 20 μm (applies to all presented images). **G)** Human motoneurons were exposed to increasing doses of glutamate for 48 hours and then fixed and stained for

Citation: James J Hickman et al. Ijppr.Human, 2017; Vol. 11 (1): 348-374.

359

neurofilament (green) and DAPI (blue). Scale bar = 30 μm. **H)** Quantification of axonal varicosities (normalized by axonal length) formed with increasing glutamate treatment. At least 30 images were collected from each condition, and conditions were compared statistically with One-way ANOVA followed by Dunnett's test. *$P < 0.01$, **$P < 0.001$; Data represents the mean ± S.E.M.

In vitro glutamate varicosity induction was reversed by reformulation of the DP

Axonal varicosities are an early axonal pathology caused by various insults to neurons and axonal neuropathy has been observed in early stage of ALS pathology (31, 40, 55, 56). To test the Deanna protocol's effectiveness in ameliorating the varicosities induced by glutamate exposure, hMNs were either simultaneously treated with glutamate and the DP formulation (listed in Figure 3A), or were exposed to a 48 hours glutamate treatment and then the DP formulation was subsequently applied for another 48 hours (Figure 3B). The DP formulation was evaluated by counting the reduction in the number of axonal varicosities formed, through immunolabelling with neurofilament, for 10 mM glutamate treated hMNs and compared to the untreated hMN controls. The treatment with the complete DP formulation (DP-1) did not change the number of axonal varicosities in either simultaneous administration or sequential treatment.

In an attempt to further evaluate the effect of the DP on varicosity formation, the effect of each DP component in the reduction of varicosities formed in glutamate treated hMNs was tested. To accomplish this, each component was systematically removed and each new formulation was tested and significant reductions were achieved with two reformulations. Elimination of either Coenzyme Q10 (CoQ10) or Nicotinic acid (NA) reduced varicosity formation significantly (Treated vs. Untreated *$P<0.05$)* (Figure 3C).

Citation: James J Hickman et al. Ijppr.Human, 2017; Vol. 11 (1): 348-374.
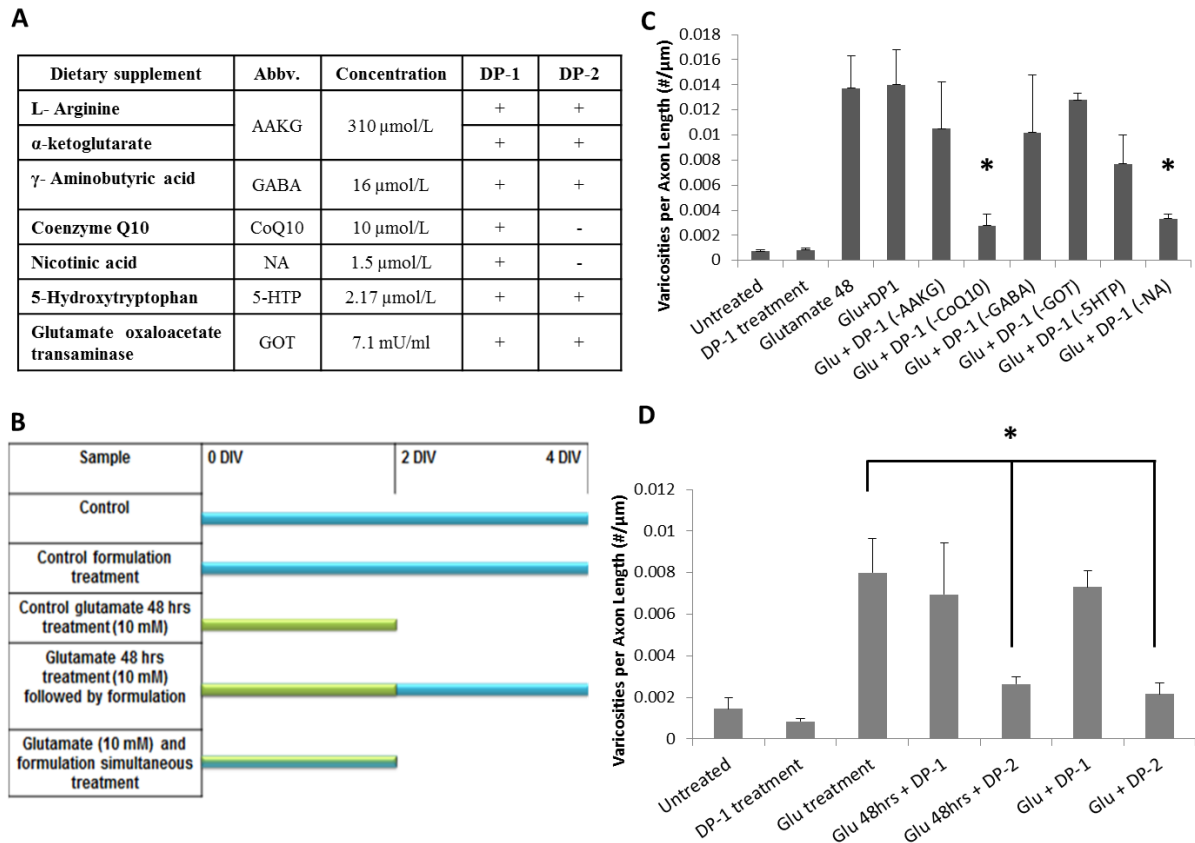
360

Figure 3. Response of glutamate treated cultures to the DP formulations. A) Formulations of DP-1 and DP-2. **B)** Schematic diagram of each hMN DP formulation treatment. **C)** Glutamate excitotoxicity was not reduced by DP-1, but by eliminating either CoQ10 and/or nicotinic acid. Following glutamate and DP treatment, hMNs were fixed and stained for neurofilament and DAPI. The number of varicosities per μm of axonal length was calculated from the collected images. At least 30 images were collected from each condition. One Way ANOVA followed by Dunnett's test was used to compare DP treatments to Glutamate 48 hour treatment (same for D). Glutamate treatment for 48 hours was different from both untreated and DP-1 treated controls ($p < 0.01$). Glu+DP-1 (-CoQ10), and Glu +DP-1 (-NA) are both significantly different from glutamate only treatment (*$p < 0.05$). **D)** Simultaneous removal of coenzyme Q10 and nicotinic acid from the DP-1 formulation reduced the number of varicosities to basal levels. Sequential treatment (Glutamate 48 hours + DP-2), and simultaneous treatment ((Glutamate +DP-2) for 48 hours) are both significantly different than glutamate treatment (*$P < 0.05$); Data represents the mean ± S.E.M.

Citation: James J Hickman et al. Ijppr.Human, 2017; Vol. 11 (1): 348-374.

361

Considering that the individual removal of CoQ10 and NA could reduce the number of axonal varicosities formed, further testing was performed for a formulation where both supplements were eliminated (Figure 3D). The removal of CoQ10 and NA produced a significant reduction on the number of axonal varicosities formed per micrometer of axonal length (Treated vs. untreated P<0.05). Furthermore, the number of varicosities returned to basal levels in either simultaneous treatment or sequential treatment, with no significant difference compared to the untreated controls (Treated vs. untreated *P>0.05*). This strongly suggests the modified DP (DP-2) (Figure 3D) can reduce, if not eliminate, the pathology induced by glutamate and gives an indication of mechanism for the disease when the anecdotal clinical evidence is considered.

Treatment of human ALS SOD1 MN phenotype with the DP-2.

While the findings from the glutamate toxicity model were exciting, they still could be unrelated to the pathology of the ALS phenotype. To address this question, iPSCs derived from hMNs containing the SOD1 mutation were tested with the DP-2 protocol. This would provide additional evidence for the DP-2 results by demonstrating correlation of the *in vitro* model with the human disease phenotype, and give stronger clinical validation for controlled testing with ALS patients.

To investigate this additional hypothesis, MNs were differentiated from an IPSC line derived from an ALS patient with the SOD1 mutation, as well as from an iPSC line (WT) derived from a normal subject. The differentiated culture was characterized by immunocytochemistry with MN markers HB9, Islet1 and SMI32, and more than 90% of the neurons were MNs (Supplemental Figure S2). Electrophysiological analysis was conducted for these ALS-hMN mutants to determine if the level of maturity reached was similar to the control hMNs. No significant differences were identified from the patch-clamp analysis of D10-D16 cultures (Figure 4A-D) in iPSC-MNs compared to the SCSC-MNs. The electrophysiological properties of the mutant iPSCs MNs were also compared to the WT iPSCs MNs and no significant differences were observed as shown in the first two rows of Table 2. Similarly, no significant differences were observed after DP-2 treatment as shown in the bottom row of Table 2.

Citation: James J Hickman et al. Ijppr.Human, 2017; Vol. 11 (1): 348-374.

362

Table 2. Analysis of the major electrophysiological parameters indicated no major differences between WT MNs and SOD-1 MNs with and without DP-2 treatment. (Data are expressed as mean ± standard deviation).

iPSC-hMNs		RP (mV)	AP (mV)	Inward Current (pA)	Outward Current (pA)	Neurons w/ repetitive firing	Rate of Repetitive Firing (Hz)
ND41865 (Wild Type)	Control	-57.17+/-9.3	87.26+/-17.8	1407+/-1230.7	943.05+/-571.1	100%	17+/-1.41
ND39032 (SOD1)	Untreated	-54.47+/-5.1	88.71+/-14.36	2327.03+/-1228.1	1247.36+/-598.3	100%	14.8+/-7.2
	DP-2	-49.67+/-9.2	80.65+/-12.46	1076.7+/-639.1	720.3+/-469.3	100%	18.3+/-3.8

Morphological analysis of the hMNs was also performed as previously described for control SCSC-hMNs for both the SOD1 mutant as well as the WT neurons (Supplemental Figure S3). For consistency with the analysis in SCSC-MNs, both WT and SOD1 iPSCs-MNs were immunostained with neurofilament antibody for quantification of axonal varicosities and co-stained with the MN marker SMI32 to confirm the identity of neurons used for quantification (Supplemental Figure S3). The left panel of Figure 4E clearly indicates few varicosities were observed in iPSC derived WT-hMNs while significant numbers of varicosities were present in the axons of the SOD1-MNs without any glutamate treatment as shown in the middle panel of Figure 4E. Immunostaining confirmed SV2 clusters in the varicosities formed in the mutant iPSCs as well (Figure 4F). The quantification of neurofilament-positive axonal varicosities in the differentiated SOD1-hMN cultures indicates that they were significantly higher than that of the WT-hMNs (Figure 4G), suggesting that axonal deficits are also present in the hMNs with the SOD1 mutation after hMN maturation.
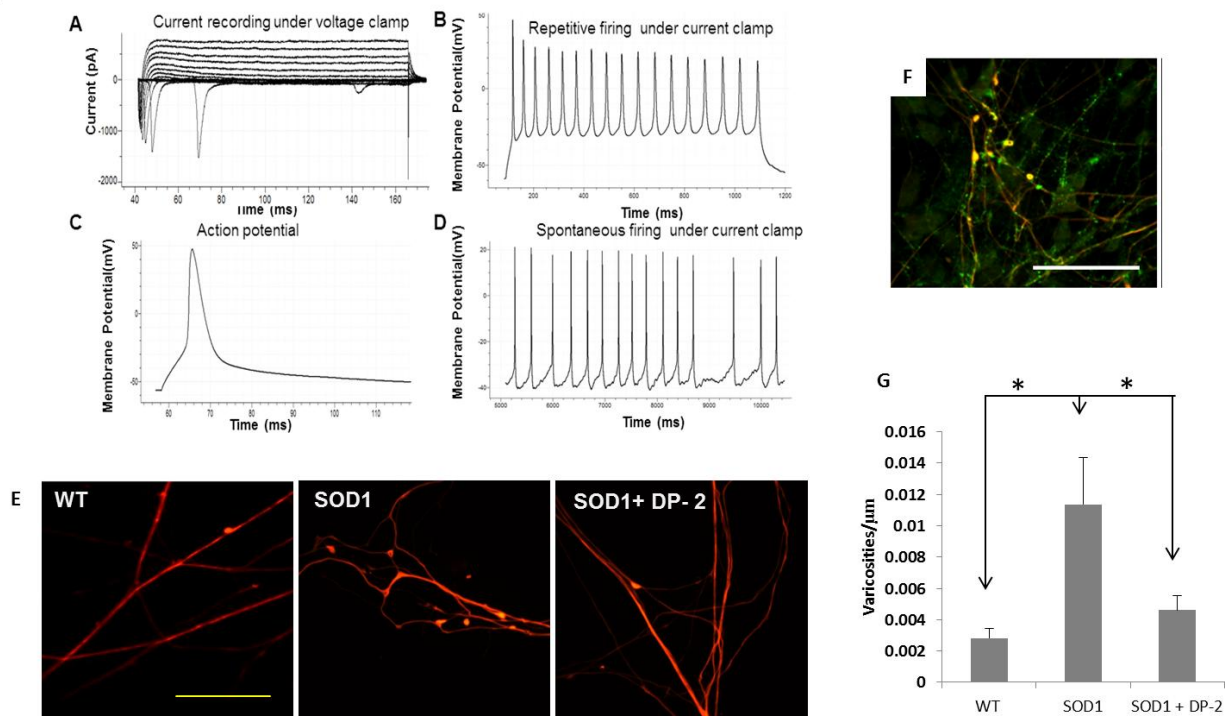
Citation: James J Hickman et al. Ijppr.Human, 2017; Vol. 11 (1): 348-374.

363

Figure 4. Electrophysiological and morphological analysis of SOD1 patient hMNs with and without DP-2 treatment. A-D) Sample traces of patch clamp recordings from SOD1 MNs. **E)** iPSC-hMNs stained for neurofilament (red) for wild type, SOD1 and SOD1 after treatment with the DP-2. **F)** SOD1-hMN at 25 Days in culture stained with NF (red) and SV2 (green) demonstrated pathological varicosities observed in the axons of these MNs and clustering of SV2 in these varicosities. Scale bar: 50 μm. **G)** Quantification of axonal varicosities (normalized to axonal length) in SOD1-hMNs with and without treatment with the DP-2. SOD1 is significantly different from WT (p=0.02) and SOD1 after DP-2 treatment (p=0.04), while WT and SOD1+DP-2 are not different (p=0.5). *P < 0.05. One Way ANOVA. Data represent the mean ± S.E.M.

In order to determine whether the DP-2 could reverse the axonal varicosities observed in the SOD1-MNs, the cells were treated with the DP-2 as above for 48 hours, and the electrophysiological properties of the treated cells were measured and the number of axonal varicosities was quantified. No significant differences were noted in the electrophysiological properties of DP-2 treated and untreated SOD1-MNs (Table 1). However, as shown in the last panel of Figure 4E and quantified in Figure 4G, the number of axonal varicosities was significantly reduced after the DP-2 treatment, indicating the effectiveness of the DP-2 not only for reducing the glutamate induced varicosities but also those present in MNs derived from a fully differentiated human mutant phenotype.

Citation: James J Hickman et al. Ijppr.Human, 2017; Vol. 11 (1): 348-374.

364

In using two vastly different lines to show similar responses of varicosities to the DP-2 treatment, clonal variation is accounted for in the fact that the population of combined spinal cord stem cell derived motoneurons and SOD1 motoneurons include the variation within each subpopulation. We show that even with the variability between two substantially different cell lines with varicosities produced from two completely different protocols, the effect of DP-2 on varicosities remains similar. By showing significant reductions in varicosities produced by two very different experimental protocols (induced and natively produced), we conclusively demonstrate that the DP-2 Deanna Protocol affects an underlying mechanism for varicosity production or prevention utilizing only one mutant cell line.

In order to be able to claim that varicosities are caused by the SOD1 mutation itself, or to claim a difference in the effectiveness of a treatment (e.g. DP-2) due to the SOD1 mutation, multiple cell lines for each condition would need to be used to isolate the effect of the SOD1 mutation. However, this work focuses on the effect of the presented treatment on the varicosities, instead of the effect of SOD1 mutations on some measured output. A mutant SOD1 line is included to demonstrate that the effect of DP-2 on varicosities is neither peculiar to a specific wild type line nor peculiar to varicosities produced by glutamate addition.

DISCUSSION

This study directly links glutamate toxicity to axonal varicosities as a possible mechanism for initial ALS progression. In addition, a metabolic treatment was shown to reduce the varicosities, providing experimental evidence to support anecdotal reports from ALS patients after this holistic treatment. The findings that significant axonal varicosity pathology occurs prior to loss of electrophysiological function or loss of hMN viability indicate it is an early disease phenotype. The presence of the varicosities in functional hMNs derived from iPSCs from SOD1 ALS patients without glutamate treatment is also in agreement with this conclusion. Reversal of these varicosities by DP treatment reveals a potential therapy for this early stage of ALS pathology.

Two major cellular pathologies have been widely observed in the study of ALS: excitotoxicity and deficit in axonal transport. Glutamate-related excitotoxicity has been frequently reported in both sporadic and familial ALS patients based on the excitotoxicity analysis of the plasma or CSF fluid (57, 58). In addition, cytoskeletal pathology, especially

Citation: James J Hickman et al. Ijppr.Human, 2017; Vol. 11 (1): 348-374.

365

axonopathy, is an important hallmark in several neurodegenerative diseases and is considered to be an early indicator for cells under extracellular or intracellular stress (59, 60). The accumulation of neurofilament, organelles and vesicles along the axons was previously reported in rat and tissue models of ALS, however never directly associated with glutamate excitotoxicity (31,40,55, 56). Impaired axonal transport has been observed in early stages of ALS pathology and correction of this deficit can significantly extend the lifespan of SOD1 mice (31, 40, 55, 56,61, 62). Especially, a study in MNs derived from iPSCs of ALS patients demonstrated that the mutant SOD1 gene can misregulate neurofilament balance and cause axonal varicosities which was then followed by neurite degeneration, and correction of the neurofilament phenotype mitigated neural degeneration (53). Impairment of axonal transport would also result in subsequent gradual loss of NMJ function which mirrors clinical observations of a gradual loss of muscle strength preceded by dysfunction (63), the typical phenotype of human ALS disease progression. Glutamate excitotoxicity can cause distal axonopathy (40) and slow neurofilament-mediated axonal transport (64). Additionally, glutamate excitotoxicity in another study was found to slow neurofilament-mediated axonal transport in a human adrenal cortex cell line SW-13 (64). The deficit can be reversed by Riluzole (31), the only FDA-approved drug for ALS which effect is at least partially due to interference with glutamate-mediated toxicity (65, 66).

In this paper, we reproduced the glutamate-induced axonal pathology in hMNs in a dose-respondent manner. Increased concentration of glutamate induced a higher density of axonal varicosities in hMNs, which were demonstrated by neurofilament clusters. The increased number of SV2 aggregates and their frequent co-localization with neurofilament clusters indicated the transportation of synaptic vesicles or related proteins would probably be hindered at these varicosities, which indicates the interruption of axonal transportation, which agrees with previous reports concerning the role of neurofilament cluster formation in inhibiting axonal transport of distal proteins (67). Considering the commonality of glutamate toxicity and axonal pathology in ALS, and the relationship between these two phenotypes, the findings from this study should be applicable for a large portion of ALS cases.

Despite the axonal neurofilament phenotype, both Glutamate-treated spinal MNs or iPSC-derived SOD1 MNs can elicit APs under depolarization or by spontaneous activity, and no significant electrophysiological deficit was detected. This could be due to axonal varicosities being an early hallmark of the pathology which may occur significantly before functional

Citation: James J Hickman et al. Ijppr.Human, 2017; Vol. 11 (1): 348-374.

366

deficits can be detected. Both hypoexcitability (68, 69) and hyperexcitability (38) phenotypes have been reported in ALS MNs, but no electrophysiological phenotype was observed in this study. This could be because the assay employed, patch clamp, is not sensitive enough to detect deficit in axonal transport at this stage of pathology.

However, the key result in this study is the ability of a holistic treatment DP, developed for ALS patients from compounds generally recognized as safe that had previously shown anecdotal evidence of patient benefit, to reverse the pathology. The subset of compounds labeled DP-2 not only reversed varicosities in the glutamate treated MNs, but also in SOD1 mutants derived from ALS patients. This is critically important based on recent results that suggest protein misfolding may be a root cause of the disease for both familial and sporadic forms (70). Two hMN cellular models for ALS were utilized in this study: SCSC- MNs exposed to glutamate and ALS patient-derived mutant MNs. The former was chosen because glutamate-related excitotoxicity has been frequently reported for both sporadic and familial ALS patients based on analysis of their plasma or CSF (57, 58). To mimic the excitotoxicity as *in vivo*, 10 mM glutamate was applied to the hMN culture for 48 hours. This concentration is higher than the regular glutamate concentration in human CSF, which has been reported to be between 0.02-20 μM depending on the technology employed to make the measurement (71). However in the synaptic cleft, glutamate concentrations can reach the millimolar level (72), and a concentration of 10 mM has been used to activate neurons during in vitro electrophysiological recordings (72). When applied to human stem cells-derived MNs in this study, this concentration was high enough to induce axonal varicosities after 48 hours exposure but low enough to not impair the electrophysiological function of the MNs, for up to 4 days after treatment justifying its choice to generate the glutamate toxicity model.

The importance of this excitotoxicity model is further confirmed by the fact that Riluzole, the only FDA-approved drug for ALS, works partially by interfering with glutamate-mediated toxicity (65, 66). In addition, due to the development of iPSC technology, patient-derived cells are now available to model disease etiology and develop therapeutics. By combining these two approaches for *in vitro* ALS modeling, findings about the cellular pathology and any drug tested would give more representative data for eventual clinical applications.

Multiple hypotheses have been proposed for the mechanisms for glutamate hypertoxicity and ultimate MN death in ALS, for example, intracellular oxidative stress and mitochondrial impairment, excessive calcium and sodium influx, from which arises mitochondrial

Citation: James J Hickman et al. Ijppr.Human, 2017; Vol. 11 (1): 348-374.

367

dysfunction, generation of free radicals and programmed cell death (6, 36). However, ALS has also been defined as a distal axonopathy by others (73, 74), and many molecular changes influencing MN degeneration occur at the NMJ at very early stages of the disease prior to symptomatic onset (9). Our study demonstrated that with the tested protocol, glutamate-induced excitotoxicity promoted axonal deformation. However, it did not affect the MN viability, significantly affect the electrophysiological function of the hMNs in culture, or cause delayed apoptosis. Due to the fact that synaptic function relies heavily on axon transport (i.e. the transport of synaptic vesicles, mitochondria etc.), glutamate induced axonopathy would cause impaired NMJ function and stability, as evidenced by typical clinical measurement in ALS patients, such as Muscle Fiber Conduction Velocity (MFCV) (9) and loss of NMJ synapses will eventually lead to MN death (8, 12, 75). These results suggest that glutamate-induced failures in axonal transport might be an early event in ALS pathology and may be an explanation of why distal structures break down first in ALS patients. Based upon our finding and the extensive literature, our hypothesis is that ALS first is induced by transport disruption which emphasizes gradual loss of function, then loss of NMJ function, then cell death as a secondary effect due to loss of retrograde feedback mechanisms such as trophic support from the muscle.

So far, very few therapeutic options for ALS patients exist, and Riluzole, the only FDA approved therapeutic, provides an improvement in patient's survival and motor function. While the neuroprotective mechanism of Riluzole action is not completely understood, it is found to be able to counteract the hyperactivity of MNs and to be related with the anti-glutamatergic properties for glutamate uptake, release and receptor signaling (76). Other therapeutics have been suggested in ALS, mainly targeting pathways known to be altered in pathological conditions, such as antioxidant activity, protein aggregation, and energy metabolism, but so far none of them have been efficacious or reproducible in clinical trials. The benefits of the DP as an ALS therapeutic have not been clinically demonstrated yet and only anecdotal reports in humans exist (http://winningthefight.org/t/Deanna-Protocol).

Using this model of glutamate toxicity in hMNs, we demonstrated that the toxicity of glutamate could be ameliorated through the use of dietary supplements. The DP did not show any effect in either simultaneous treatment or sequential treatment. The DP-2, formed by eliminating CoQ10 and nicotinic acid, reversed the varicosity phenotype to basal levels in both glutamate treated WT-MNs and iPSC ALS-MNs. CoQ10 and nicotinic acid are both

Citation: James J Hickman et al. Ijppr.Human, 2017; Vol. 11 (1): 348-374.

368

involved in citric acid metabolism and energy production. Considering the fact that NA is metabolically converted to NADH and NADPH (1, 77-79) and CoQ10 has a rapid uptake by the liver (80), and actual plasma levels could be much lower, these two components could potentially be beneficial if the metabolites (NADH & NADPH) of NA, or a reduced dosage for CoQ10, in the in vitro testing were utilized instead.

This proposed early disease phenotype is supported by previous work in animal models where treatments to protect or rescue MNs did not extend animal life (81, 82). In addition, the harmful effect of glutamate and the therapeutic effect of Glutamate Oxaloacetate Transaminase (GOT) supports the reported role of astrocytes in the pathology as they are responsible for uptake of excess glutamate (14, 83, 84). The overall conclusion of the study results demonstrates that lower levels of glutamate which would be present initially can cause functional deficits while higher levels would lead to cell death, which would follow known disease pathology.

CONCLUSIONS

The reversibility of axonal varicosity formation implies that treatment at this early stage can provide an effective therapy for ALS. Therefore, abnormal axonal transport represents not only an early detectable marker for ALS pathology but also a therapeutic target in ALS drug screening. Familial ALS represents only about 10% of all ALS cases. SOD1 gene mutation is responsible for about 10~20% of fALS. More than 100 SOD1 mutations have been linked to fALS and each causes different degrees of disease severity (85). It is possible that the early axonal varicosity phenotype may not happen in all ALS cases. However, initial neuromuscular junction failure at the onset of all ALS cases suggests that the defective distant communication between MN soma and its axonal terminal at an early stage could be an important mechanism for ALS etiology, and this communication relies on axonal transport. The commonality of this early stage axonal abnormality can be better addressed after analyzing more ALS subtypes with patient-derived MNs.

Each component of the DP-2 formulation also needs to be analyzed and the treatment optimized for clinical benefit as the original compounds were assembled to treat a metabolic disease, not protein aggregation. In addition, functional studies in a NMJ system (46) need to be carried out to confirm the connection between varicosity formation and impairment of

Citation: James J Hickman et al. Ijppr.Human, 2017; Vol. 11 (1): 348-374.

369

muscle activity. Once this is in place, efforts could then proceed for restoration of function in conjunction with other treatments, such as stem cell therapy.

ACKNOWLEDGMENTS:

REFERENCES

1. Ari C, Poff AM, Held HE, Landon CS, Goldhagen CR, Mavromates N, et al. Metabolic therapy with Deanna Protocol supplementation delays disease progression and extends survival in amyotrophic lateral sclerosis (ALS) mouse model. PLoS One. 2014;9(7):e103526.

2. Turner MR, Bowser R, Bruijn L, Dupuis L, Ludolph A, McGrath M, et al. Mechanisms, models and biomarkers in amyotrophic lateral sclerosis. Amyotroph Lateral Scler Frontotemporal Degener. 2013;14(Suppl 1):19-32.

3. Ajroud-Driss S, Siddique T. Sporadic and hereditary amyotrophic lateral sclerosis (ALS). Biochim Biophys Acta. 2015;1852(4):679-84.

4. Manfredi G, Xu Z. Mitochondrial dysfunction and its role in motor neuron degeneration in ALS. Mitochondrion. 2005;5(2):77-87.

5. Choi DW. Glutamate neurotoxicity and diseases of the nervous system. Neuron. 1988;1(8):623-34.

6. Dong XX, Wang Y, Qin ZH. Molecular mechanisms of excitotoxicity and their relevance to pathogenesis of neurodegenerative diseases. Acta Pharmacol Sin. 2009;30(4):379-87.

7. Zhang LN, Hao L, Wang HY, Su HN, Sun YJ, Yang XY, et al. Neuroprotective effect of resveratrol against glutamate-induced excitotoxicity. Adv Clin Exp Med. 2015;24(1):161-5.

8. Fischer LR, Culver DG, Tennant P, Davis AA, Wang M, Castellano-Sanchez A, et al. Amyotrophic lateral sclerosis is a distal axonopathy: evidence in mice and man. Exp Neurol. 2004;185(2):232-40.

9. Moloney EB, de Winter F, Verhaagen J. ALS as a distal axonopathy: molecular mechanisms affecting neuromuscular junction stability in the presymptomatic stages of the disease. Front Neurosci. 2014;8.

10. Dupuis L, Loeffler J-P. Neuromuscular junction destruction during amyotrophic lateral sclerosis: insights from transgenic models. Curr Opin Pharmacol. 2009;9(3):341-6.

11. Bruneteau G, Bauché S, Gonzalez de Aguilar JL, Brochier G, Mandjee N, Tanguy M-L, et al. Endplate denervation correlates with Nogo-A muscle expression in amyotrophic lateral sclerosis patients. Ann Clin Transl Neurol. 2015;2:362-72.

Citation: James J Hickman et al. Ijppr.Human, 2017; Vol. 11 (1): 348-374.

370

12. Jokic N, Gonzalez de Aguilar JL, Dimou L, Lin S, Fergani A, Ruegg MA, et al. The neurite outgrowth inhibitor Nogo-A promotes denervation in an amyotrophic lateral sclerosis model. EMBO Rep. 2006;7(11):1162-7.

13. Di Giorgio FP, Carrasco MA, Siao MC, Maniatis T, Eggan K. Non-cell autonomous effect of glia on motor neurons in an embryonic stem cell-based ALS model. Nat Neurosci. 2007;10(5):608-14.

14. Maragakis NJ, Rothstein JD. Mechanisms of Disease: astrocytes in neurodegenerative disease. Nat Clin Pract Neurol. 2006;2:679-89.

15. Phatnani HP, Guarnieri P, Friedman BA, Carrasco MA, Muratet M, O'Keeffe S, et al. Intricate interplay between astrocytes and motor neurons in ALS. Proc Natl Acad Sci USA. 2013;110:E756-65.

16. Pirooznia SK, Dawson VL, Dawson TM. Motor neuron death in ALS: programmed by astrocytes. Neuron. 2014;81:961-3.

17. Boillee S, Yamanaka K, Lobsiger CS, Copeland NG, Jenkins NA, Kassiotis G, et al. Onset and Progression in Inherited ALS Determined by Motor Neurons and Microglia. Science. 2006;312(5778):1389-92.

18. Hall ED, Oostveen JA, Gurney ME. Relationship of microglial and astrocytic activation to disease onset and progression in a transgenic model of familial ALS. Glia. 1998;23:249-56.

19. Henkel JS, Engelhardt JI, Siklós L, Simpson EP, Kim SH, Pan T, et al. Presence of dendritic cells, MCP-1, and activated microglia/macrophages in amyotrophic lateral sclerosis spinal cord tissue. Ann Neurol. 2004;55:221-35.

20. Henkel JS, Beers DR, Zhao W, Appel SH. Microglia in ALS: the good, the bad, and the resting. J Neuroimmune Pharmacol. 2009;4(4):389-98.

21. Kawamata T, Akiyama H, Yamada T, McGeer PL. Immunologic reactions in amyotrophic lateral sclerosis brain and spinal cord tissue. Am J Pathol. 1992;140:691-707.

22. Papadeas ST, Kraig SE, O'Banion C, Lepore AC, Maragakis NJ. Astrocytes carrying the superoxide dismutase 1 (SOD1G93A) mutation induce wild-type motor neuron degeneration in vivo. Proc Natl Acad Sci U S A. 2011;108(43):17803-8.

23. Zhao W, Beers DR, Appel SH. Immune-mediated mechanisms in the pathoprogression of amyotrophic lateral sclerosis. J Neuroimmune Pharmacol. 2013;8:888-99.

24. Fournier C, Bedlack B, Hardiman O, Heiman-Patterson T, Gutmann L, Bromberg M, et al. ALS Untangled No. 20: the Deanna protocol. Amyotroph Lateral Scler Frontotemporal Degener. 2013;14(4):319-23.

25. Renton AE, Majounie E, Waite A, Simón-Sánchez J, Rollinson S, Gibbs JR, et al. A hexanucleotide repeat expansion in C9ORF72 is the cause of chromosome 9p21-linked ALS-FTD. Neuron. 2011;72(2):257-68.

26. Kent L, Vizard TN, Smith BN, Topp SD, Vance C, Gkazi A, et al. Autosomal dominant inheritance of rapidly progressive amyotrophic lateral sclerosis due to a truncation mutation in the fused in sarcoma (FUS) gene. Amyotroph Lateral Scler Frontotemporal Degener. 2014;15:557-62.

27. Saris CG, Groen EJ, van Vught PW, van Es MA, Blauw HM, Veldink JH, et al. Gene expression profile of SOD1-G93A mouse spinal cord, blood and muscle. Amyotroph Lateral Scler Frontotemporal Degener. 2013;14:190-8.

28. Vanden Broeck L, Callaerts P, Dermaut B. TDP-43-mediated neurodegeneration: towards a loss-of-function hypothesis. Trends in Molecular Medicine. 2014;20(2):66-71.

29. Fischer-Hayes LR, Brotherton T, Glass JD. Axonal degeneration in the peripheral nervous system: implications for the pathogenesis of amyotrophic lateral sclerosis. Exp Neurol. 2013;246:6-13.

30. Highley JR, Kirby J, Jansweijer JA, Webb PS, Hewamadduma CA, Heath PR, et al. Loss of nuclear TDP-43 in amyotrophic lateral sclerosis (ALS) causes altered expression of splicing machinery and widespread dysregulation of RNA splicing in motor neurones. Neuropathol Appl Neurobiol. 2014;40(6):670-85.

31. Stevenson A, Yates DM, Manser C, De Vos K, Vagnoni A, Leigh PN, et al. Riluzole protects against glutamate-induced slowing of neurofilament axonal transport. Neurosci Lett. 2009;454(2):161-4.

32. Ciechanover A, Kwon YT. Degradation of misfolded proteins in neurodegenerative diseases: therapeutic targets and strategies. Exp Mol Med. 2015;47:e147.

33. Ikenaka K, Kawai K, Katsuno M, Huang Z, Jiang YM, Iguchi Y, et al. dnc-1/dynactin 1 knockdown disrupts transport of autophagosomes and induces motor neuron degeneration. PLoS One. 2013;8:e54511.

34. Moughamian AJ, Holzbaur EL. Dynactin is required for transport initiation from the distal axon. Neuron. 2012;74:331-43.

Citation: James J Hickman et al. Ijppr.Human, 2017; Vol. 11 (1): 348-374.

371

35. Foerster BR, Pomper MG, Callaghan BC, Petrou M, Edden RA, Mohamed MA, et al. An imbalance between excitatory and inhibitory neurotransmitters in amyotrophic lateral sclerosis revealed by use of 3-T proton magnetic resonance spectroscopy. JAMA Neurol. 2013;70(8):1009-16.

36. Foran E, Trotti D. Glutamate transporters and the excitotoxic path to motor neuron degeneration in amyotrophic lateral sclerosis. Antioxid Redox Signal. 2009;11(7):1587-602.

37. Dorsey ER, Johnston SC, Poole M, O'Neill GN, Bebchuk J, Wittes J, et al. Clinical trials in neurology : design, conduct, analysis. Ravina B, Cummings JL, McDermott M, Poole RM, editors. Cambridge: Cambridge University Press; 2012.

38. Wainger BJ, Kiskinis E, Mellin C, Wiskow O, Han SS, Sandoe J, et al. Intrinsic membrane hyperexcitability of amyotrophic lateral sclerosis patient-derived motor neurons. Cell Rep. 2014;7(1):1-11.

39. Cozzolino M, Carri MT. Mitochondrial dysfunction in ALS. Prog Neurobiol. 2012;97(2):54-66.

40. King AE, Dickson TC, Blizzard CA, Foster SS, Chung RS, West AK, et al. Excitotoxicity mediated by non-NMDA receptors causes distal axonopathy in long-term cultured spinal motor neurons. Eur J Neurosci. 2007;26(8):2151-9.

41. Wood JD, Beaujeux TP, Shaw PJ. Protein aggregation in motor neurone disorders. Neuropathol Appl Neurobiol. 2003;29(6):529-45.

42. Xiao S, McLean J, Robertson J. Neuronal intermediate filaments and ALS: a new look at an old question. Biochim Biophys Acta. 2006;1762(11-12):1001-12.

43. Das M, Molnar P, Devaraj H, Poeta M, Hickman J. Electrophysiological and morphological characterization of rat embryonic motoneurons in a defined system. Biotechnol Prog. 2003;19:1756-61.

44. Guo X, Johe K, Molnar P, Davis H, Hickman J. Characterization of a human fetal spinal cord stem cell line, NSI-566RSC, and its induction to functional motoneurons. Journal of Tissue Engineering Regenerative Medicine. 2010;4(3):181-93.

45. Qu Q, Li D, Louis KR, Li X, Yang H, Sun Q, et al. High-efficiency motor neuron differentiation from human pluripotent stem cells and the function of Islet-1. Nat Commun. 2014;5:3449.

46. Smith AST, Long CJ, Pirozzi K, Hickman JJ. A functional system for high-content screening of neuromuscular junctions in vitro. Technology. 2013;1(1):37-48.

47. Tang-Schomer MD, Johnson VE, Baas PW, Stewart W, Smith DH. Partial interruption of axonal transport due to microtubule breakage accounts for the formation of periodic varicosities after traumatic axonal injury. Exp Neurol. 2012;233(1):364-72.

48. Tomei G, Spagnoli D, Ducati A, Landi A, Villani R, Fumagalli G, et al. Morphology and neurophysiology of focal axonal injury experimentally induced in the guinea pig optic nerve. Acta Neuropathol. 1990;80(5):506-13.

49. Johnson VE, Stewart W, Smith DH. Axonal pathology in traumatic brain injury. Exp Neurol. 2013;246:35-43.

50. Liebert AD, Chow RT, Bicknell BT, Varigos E. Neuroprotective Effects Against POCD by Photobiomodulation: Evidence from Assembly/Disassembly of the Cytoskeleton. J Exp Neurosci. 2016;10:1-19.

51. Stokin GB, Lillo C, Falzone TL, Brusch RG, Rockenstein E, Mount SL, et al. Axonopathy and Transport Deficits Early in the Pathogenesis of Alzheimer's Disease. Science. 2005;307(5713):1282-8.

52. Tesseur I, Van Dorpe J, Bruynseels K, Bronfman F, Sciot R, Van Lommel A, et al. Prominent Axonopathy and Disruption of Axonal Transport in Transgenic Mice Expressing Human Apolipoprotein E4 in Neurons of Brain and Spinal Cord. The American Journal of Pathology. 2000;157(5):1495-510.

53. Chen H, Qian K, Du Z, Cao J, Petersen A, Liu H, et al. Modeling ALS with iPSCs Reveals that Mutant SOD1 Misregulates Neurofilament Balance in Motor Neurons. Cell Stem Cell. 2014;14:796-809.

54. Feany MB, Lee S, Edwards RH, Buckley KM. The synaptic vesicle protein SV2 is a novel type of transmembrane transporter. Cell. 1992;70:861-7.

55. Mitra NK, Goh TE, Bala Krishnan T, Nadarajah VD, Vasavaraj AK, Soga T. Effect of intra-cisternal application of kainic acid on the spinal cord and locomotor activity in rats. Int J Clin Exp Pathol. 2013;6(8):1505-15.

56. Morrison BM, Shu IW, Wilcox AL, Gordon JW, Morrison JH. Early and selective pathology of light chain neurofilament in the spinal cord and sciatic nerve of G86R mutant superoxide dismutase transgenic mice. Exp Neurol. 2000;165(2):207-20.

Citation: James J Hickman et al. Ijppr.Human, 2017; Vol. 11 (1): 348-374.

372

57. Van Den Bosch L, Van Damme P, Bogaert E, Robberecht W. The role of excitotoxicity in the pathogenesis of amyotrophic lateral sclerosis. Biochimica et Biophysica Acta (BBA) - Molecular Basis of Disease. 2006;1762(11–12):1068-82.

58. Heath PR, Shaw PJ. Update on the glutamatergic neurotransmitter system and the role of excitotoxicity in amyotrophic lateral sclerosis. Muscle Nerve. 2002;26(4):438-58.

59. Coleman M. Axon degeneration mechanisms: commonality amid diversity. Nat Rev Neurosci. 2005;6(11):889-98.

60. Vos KJD, Grierson AJ, Ackerley S, Miller CCJ, PM A-S, MM M, et al. Role of Axonal Transport in Neurodegenerative Diseases_Expanding insights of mitochondrial dysfunction in Parkinson's disease. Annu Rev Neurosci. 2008;31(1):151-73.

61. Kieran D, Hafezparast M, Bohnert S, Dick JR, Martin J, Schiavo G, et al. A Mutation in Dynein Rescues Axonal Transport Defects and Extends the Life Span of ALS Mice. J Cell Biol. 2005;169(4):561-7.

62. Williamson TL, Cleveland DW. Slowing of axonal transport is a very early event in the toxicity of ALS-linked SOD1 mutants to motor neurons. Nat Neurosci. 1999;2(1):50-6.

63. Gordon PH. Amyotrophic Lateral Sclerosis: An update for 2013 clinical features, pathophysiology, management and therapeutic trials. Aging Dis. 2013;4(5):295-310.

64. Ackerley S, Grierson AJ, Brownlees J, Thornhill P, Anderton BH, Leigh PN, et al. Glutamate Slows Axonal Transport of Neurofilaments in Transfected Neurons. J Cell Biol. 2000;150(1):165-76.

65. Lacomblez L, Bensimon G, Leigh PN, Guillet P, Meininger V. Dose-ranging study of riluzole in amyotrophic lateral sclerosis Amyotrophic Lateral Sclerosis/Riluzole Study, Group II. Lancet. 1996;347(9013):1425-31.

66. Ludolph AC, Meyer T, Riepe MW. The role of excitotoxicity in ALS – what is the evidence? J Neurol. 2000;247(1):I7-I16.

67. Julien JP, Cote F, Collard JF. Mice overexpressing the human neurofilament heavy gene as a model of ALS. Neurobiology of Aging. 1995;16(3):487-90.

68. Sareen D, O'Rourke JG, Meera P, Muhammad AKMG, Grant S, Simpkinson M, et al. Targeting RNA foci in iPSC-derived motor neurons from ALS patients with a C9ORF72 repeat expansion. Sci Transl Med. 2013;5(208):208ra149.

69. Zhang Z, Almeida S, Lu Y, Nishimura AL, Peng L, Sun D, et al. Downregulation of MicroRNA-9 in iPSC-Derived Neurons of FTD/ALS Patients with TDP-43 Mutations. PLoS One. 2013;8:e76055.

70. Rotunno MS, Bosco DA. An emerging role for misfolded wild-type SOD1 in sporadic ALS pathogenesis. Front Cell Neurosci. 2013;7:110-24.

71. Moussawi K, Riegel A, Nair S, Kalivas PW. Extracellular Glutamate: Functional Compartments Operate in Different Concentration Ranges. Front Syst Neurosci. 2011;5:94.

72. Diamond JS, Jahr CE. Transporters Buffer Synaptically Released Glutamate on a Submillisecond Time Scale. The Journal of Neuroscience. 1997;17(12):4672-87.

73. Noto Y-i, Kanai K, Misawa S, Shibuya K, Isose S, Nasu S, et al. Distal motor axonal dysfunction in amyotrophic lateral sclerosis. J Neurol Sci. 2011;302(1–2):58-62.

74. Cheah BC, Lin CSY, Park SB, Vucic S, Krishnan AV, Kiernan MC. Progressive axonal dysfunction and clinical impairment in amyotrophic lateral sclerosis. Clin Neurophysiol. 2012;123(12):2460-7.

75. Boillée S, Vande Velde C, Cleveland Don W. ALS: A Disease of Motor Neurons and Their Nonneuronal Neighbors. Neuron. 2006;52(1):39-59.

76. Bellingham MC. A review of the neural mechanisms of action and clinical efficiency of Riluzole in treating Amyotrophic Lateral Sclerosis: What have we learned in the last decade. CNS Neurosci Ther. 2011;17(1):4-31.

77. Beal MF. Coenzyme Q10 administration and its potential for treatment of neurodegenerative diseases. Biofactors. 1999;9(2-4):261-6.

78. Chang Y, Huang S-K, Wang S-J. Coenzyme Q10 Inhibits the Release of Glutamate in Rat Cerebrocortical Nerve Terminals by Suppression of Voltage-Dependent Calcium Influx and Mitogen-Activated Protein Kinase Signaling Pathway. J Agric Food Chem. 2012;60(48):11909-18.

79. Li G, Zou L-Y, Cao C-M, Yang ES. Coenzyme Q10 protects SHSY5Y neuronal cells from beta amyloid toxicity and oxygen-glucose deprivation by inhibiting the opening of the mitochondrial permeability transition pore. Biofactors. 2005;25(1-4):97-107.

Citation: James J Hickman et al. Ijppr.Human, 2017; Vol. 11 (1): 348-374.

373

80. Kamanna VS, Kashyap ML. Mechanism of Action of Niacin. Am J Cardiol. 2008;101(8, Supplement):S20-S6.

81. Corona JC, Tovar-y-Romo LB, Tapia R. Glutamate excitotoxicity and therapeutic targets for amyotrophic lateral sclerosis. Expert Opin Ther Targets. 2007;11:1415-28.

82. Maragakis NJ, Jackson M, Ganel R, Rothstein JD. Topiramate protects against motor neuron degeneration in organotypic spinal cord cultures but not in G93A SOD1 transgenic mice. Neurosci Lett. 2003;338:107-10.

83. Blackburn D, Sargsyan S, Monk PN, Shaw PJ. Astrocyte function and role in motor neuron disease: a future therapeutic target. Glia. 2009;57:1251-64.

84. Brites D, Vaz AR. Microglia centered pathogenesis in ALS: insights in cell interconnectivity. Front Cell Neurosci. 2014;8:117.

85. Karumbayaram S, Kelly TK, Paucar AA, Roe AJ, Umbach JA, Charles A, et al. Human embryonic stem cell-derived motor neurons expressing SOD1 mutants exhibit typical signs of motor neuron degeneration linked to ALS. Dis Model Mech 2009;2(3-4):189-95.

Citation: James J Hickman et al. Ijppr.Human, 2017; Vol. 11 (1): 348-374.

374